MRS Bulletin

CELEBRATING 45 YEARS

MRS MATERIALS RESEARCH SOCIETY®
Advancing materials. Improving the quality of life.

February 2020 Vol. 45 No. 2
mrs.org/bulletin

Transient electronic devices

ALSO IN THIS ISSUE

Self-assembly of functional nanoscale materials

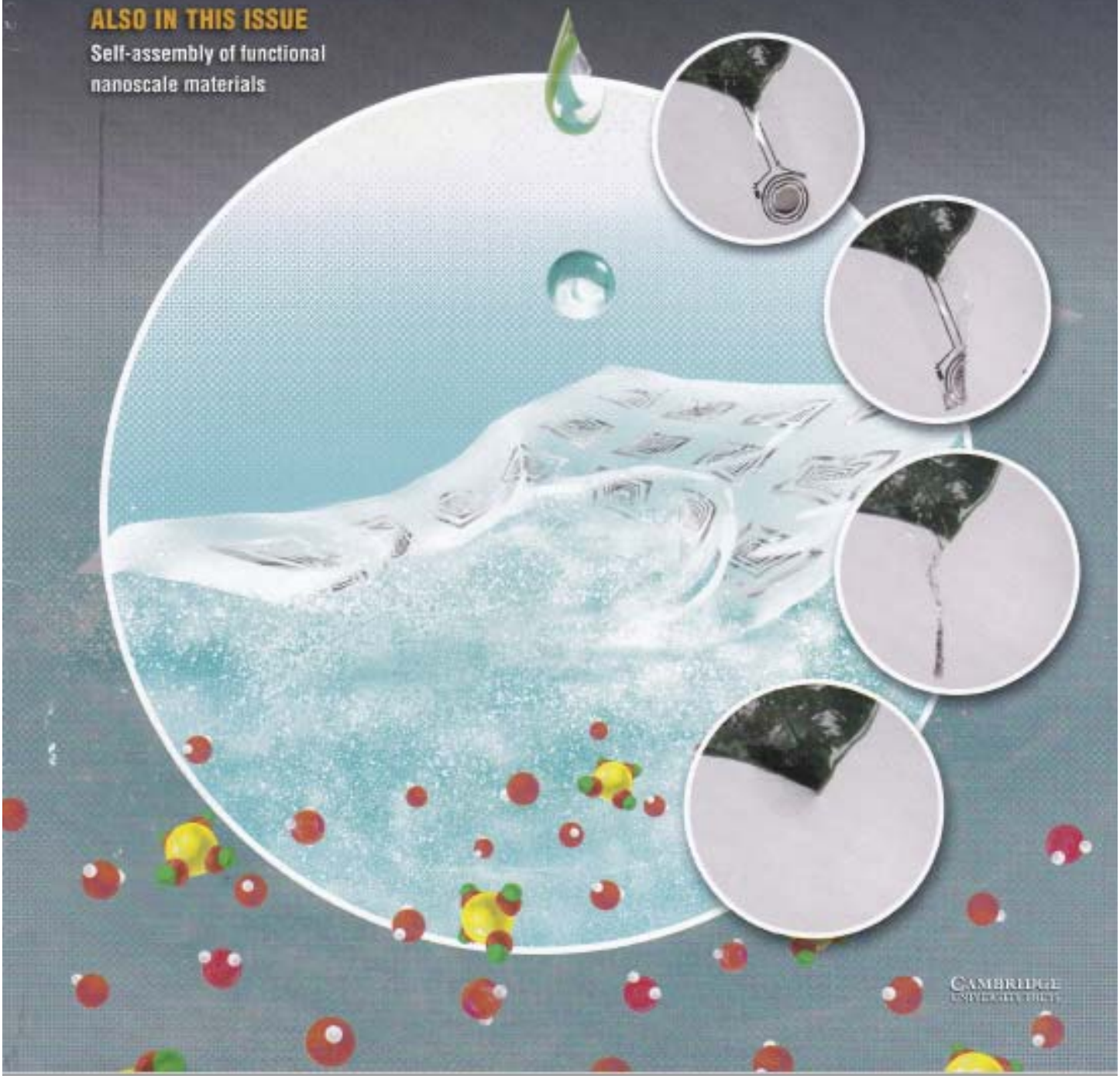

CAMBRIDGE UNIVERSITY PRESS

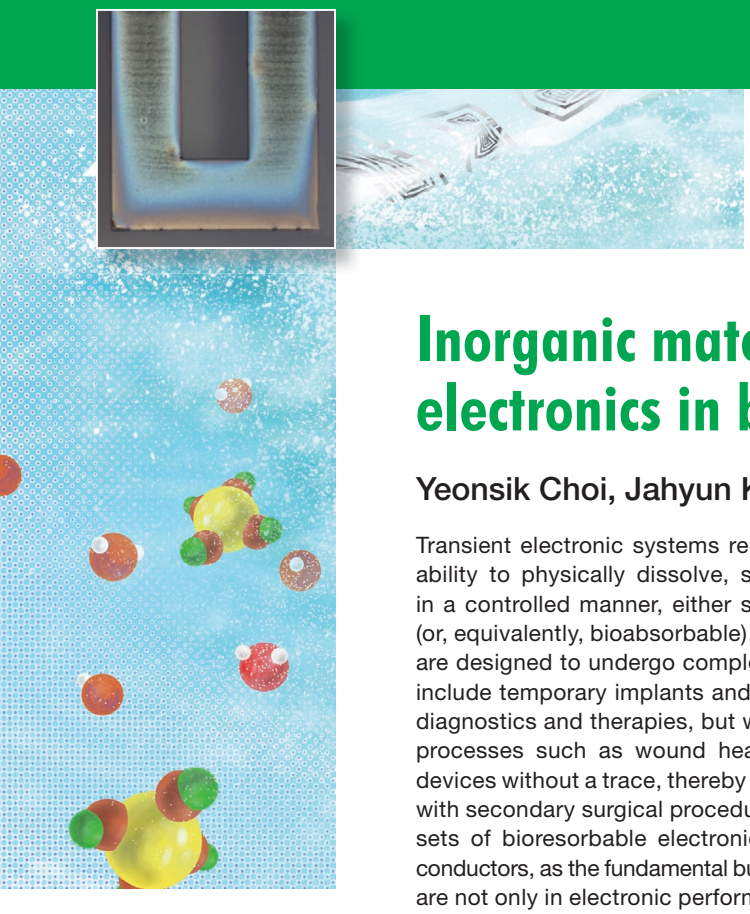

Inorganic materials for transient electronics in biomedical applications

Yeonsik Choi, Jahyun Koo, and John A. Rogers

Transient electronic systems represent an emerging class of technology defined by an ability to physically dissolve, sublime, chemically degrade, disintegrate, or transform in a controlled manner, either spontaneously or through a trigger event. Bioresorbable (or, equivalently, bioabsorbable) electronic devices, as a subset of transient technologies, are designed to undergo complete dissolution when immersed in biofluids. Applications include temporary implants and other medical devices that serve important purposes in diagnostics and therapies, but with finite lifetimes matched to those of natural biological processes such as wound healing. Here, transience by bioresorption eliminates the devices without a trace, thereby bypassing the costs, complications, and risks associated with secondary surgical procedures for device retrieval. Such systems demand complete sets of bioresorbable electronic materials, including semiconductors, dielectrics, and conductors, as the fundamental building blocks for functional components. The considerations are not only in electronic performance, but in degradation chemistry and biocompatibility of both the materials and the products of their reactions with biofluids. This article highlights recent progress in this area of materials science and describes some of the most sophisticated bioresorbable electronic systems that combine these materials with bioresorbable polymers, the biomedical applications of these devices, and some directions for future work.

Introduction

Inorganic materials are attractive choices for electronic devices that can be configured to completely and harmlessly dissolve, resorb, or degrade, at a molecular level, as temporary biomedical implants or environmental sensors.[1] **Figure 1**a shows a sequence of images of a Colpitts radio-frequency (RF) oscillator, as a source of a single-frequency RF signal that incorporates various representative bioresorbable electronic components, including inductors, capacitors, resistors, diodes, transistors, interconnects, substrates, and encapsulation layers, all of which dissolve over controlled periods of time when immersed in water.[1] The ability to use inorganic materials in these systems, including certain classes that appear in conventional, nontransient electronics, creates many opportunities for high-performance, sophisticated modes of operation and for the use of production schemes that align, at least partly, with those of established foundry facilities in the semiconductor industry. A key to the successful development of inorganic bioresorbable electronics is in understanding the fundamental aspects of the chemistry of dissolution in biofluids, and of the biocompatibility of the materials and the products of their degradation, either when used alone or together with organic bioresorbable materials.[2–4]

This article reviews these aspects in the context of the most important inorganic bioresorbable electronic materials, with a focus on those demonstrated in fully functional bioresorbable systems for specific potential applications in biomedicine. By comparison to organic alternatives, inorganics offer excellent electrical performance characteristics and the ability to operate in a stable fashion over time frames relevant to various physiological processes, such as wound healing cascades, encountered in human healthcare. In addition to an overview of the materials, we include examples of advanced devices, with capabilities in both sensing bioprocesses and delivering therapies across conditions that range from recovery from traumatic brain injury to healing of damaged peripheral nerves. We conclude with directions for future research.

Yeonsik Choi, Center for Bio-Integrated Electronics, Northwestern University, USA; yeonsik.choi@northwestern.edu
Jahyun Koo, Center for Bio-Integrated Electronics, Northwestern University, USA; nano.jhkoo@gmail.com
John A. Rogers, Biomedical Engineering and Medicine, and Institute for Bioelectronics, Northwestern University, USA; jrogers@northwestern.edu
doi:10.1557/mrs.2020.25

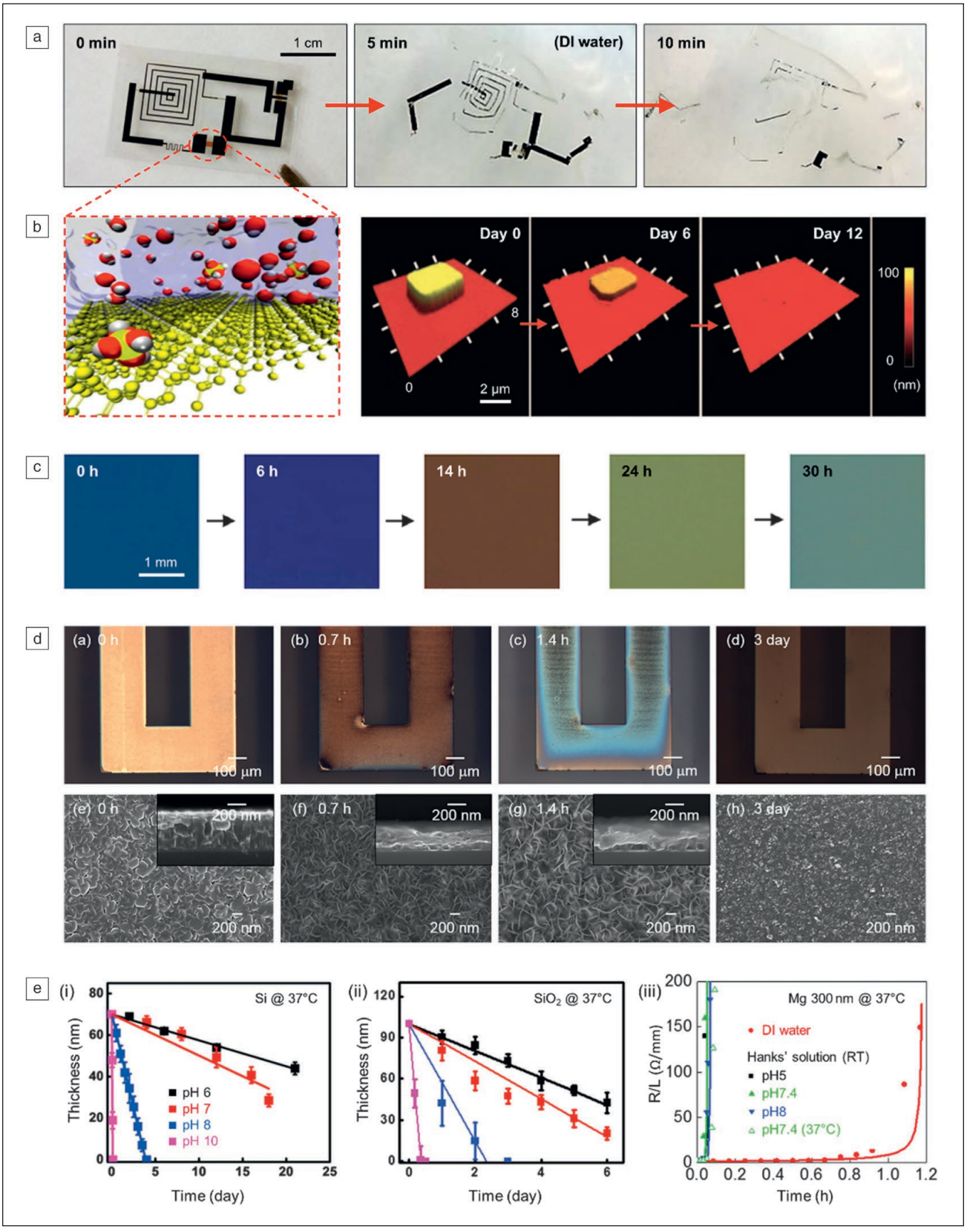

Bioresorbable inorganic electronic materials

Silicon

For electronic devices, generally, and transient technologies specifically, the semiconductor is the most challenging material component. The observation that nanoscale elements of monocrystalline silicon naturally dissolve in biofluids on time scales relevant to human healthcare applications established the foundation for high-performance classes of bioresorbable electronics.[1]

Combined experimental and theoretical studies suggest that hydrolysis represents the main chemical reaction mechanism responsible for the dissolution of silicon in aqueous media ($Si + 4H_2O \rightarrow Si(OH)_4 + 2H_2$) at near neutral pH conditions of relevance to applications in biomedicine and environmental monitoring (Figure 1b, left). Typical rates in many types of biofluids are such that this reaction runs to completion with nanometer-thick films of silicon (i.e., silicon nanomembranes [Si NMs]), over time scales of days to weeks.[5] Figure 1b (right) shows measurements of changes in the thickness of a lightly *p*-doped Si NM (initial dimensions: 3 mm × 3 mm × 70 nm) at various times of immersion in phosphate buffered saline (PBS; pH 7.4) at physiological temperature (37°C).[1] The rate of dissolution observed in this case (~5 nm/day) implies that a Si NM with thickness of 100 nm, a value typical for many electronic devices, will completely dissolve within ~20 days under these conditions.[1] Figure 1e(i) shows similar results measured for Si NMs in PBS at different pH values.[6]

In all cases, the linear relationship between thickness and time is consistent with a surface erosion reaction mechanism, without significant contribution of reactive diffusion processes. The increasing reaction rate with increasing pH suggests a nucleophilic reaction between the hydrogen-terminated Si atoms of the Si NM and OH^- groups in the surrounding fluid. Modeling identifies that one possible mechanism involves a pair of OH^- ions that react through dangling bonds at the surface of the NM to reduce the strength of Si back bonds. Breaking of these bonds then yields a silicon hydroxide complex that combines with two additional OH^- ions to produce $Si(OH)_4$.[7] As expected, increasing the concentration of OH^- accelerates the rate of the reaction. This chemistry is related to the well-known alkaline wet-etching processes for silicon, where the rate of dissolution (R) depends on the concentrations of water (H_2O) and KOH according to

$$R = k_0[H_2O]^4[OH^-]^{0.25} e^{-\left(\frac{E_A}{k_B T}\right)},$$

where k_0, E_A, k_B, and T are the reaction constant, the activation energy, the Boltzmann constant, and the temperature in Kelvin, respectively.[1] This empirical formula also suggests that the temperature dependence follows Arrhenius scaling, consistent with experimental findings.

Other chemicals present in the surrounding solution can also affect the chemistry, particularly in complex biofluids and as implants in confined geometries. For example, as the silicon dissolves, the local concentration of the $Si(OH)_4$ increases in a manner that can decrease the reaction rate. Surface adsorbed proteins can also decelerate the dissolution processes by limiting diffusive access of water.[8] In spite of the complex materials chemistry, Si NMs dissolve in a controlled manner. They can serve as the basis for high-performance, bioresorbable electronic devices, as well as various classes of sensors and other components. For example, typical bioresorbable *n*-channel metal oxide semiconductor field effect transistors ([MOSFETs]; channel length ~10 μm; channel width ~40 μm) built using Si NMs exhibit saturation mobilities, linear regime mobilities, and on/off ratios of ~530 cm^2/Vs, ~650 cm^2/Vs, and $>10^5$, respectively.[9]

Other forms of silicon and germanium

Related forms of silicon (Si) and germanium (Ge) offer alternatives to monocrystalline Si, with qualitatively similar dissolution chemistries. For instance, in aqueous media at physiological conditions (PBS; pH 7.4; 37°C), polycrystalline Si (poly-Si), amorphous Si (a-Si), Ge, and Si-Ge alloy (SiGe) dissolve at rates of 2.8, 4.1, 3.1, and 0.1 nm/day, respectively.[10] The rate for a-Si is higher than that of poly-Si largely due to its lower density, and corresponding increase in the rate of water penetration and reaction due to a lower E_A of a-Si (0.518 eV) compared to that of poly-Si (0.524 eV).[11–13] The dissolution of Ge, which has a smaller bandgap and larger minority-carrier mobility than Si, follows from similar hydrolysis mechanisms ($Ge + O_2 + H_2O \rightarrow H_2GeO_3$).[10] Poly-Si, a-Si, and Ge dissolve with a dependence on pH and temperature similar to that of monocrystalline Si due to the similar values of E_A (0.51–0.52 eV). For example, at pH 10, patterned arrays of squares (3 μm × 3 μm × 100 nm) of Si and Ge dissolve within a few

Figure 1. Chemistry and kinetics of dissolution of bioresorbable inorganic electronic materials. (a) Images of dissolution of a Colpitts oscillator constructed entirely with biodegradable electronic materials. Reprinted with permission from Reference 1. © 2012 AAAS. (b) (Left) Illustration of the reaction between the inorganic semiconductor, monocrystalline silicon, by hydrolysis during immersion in water. Reprinted with permission from Reference 8. © 2017 American Chemical Society. (Right) Series of topographical images of a Si nanomembrane (NM) at various stages of dissolution by hydrolysis following immersion in phosphate buffer solution (PBS) at physiological pH and temperature. Reprinted with permission from Reference 1. © 2012 AAAS. (c) Optical images of the inorganic dielectric, thermally grown (tg)-SiO_2, collected at several times after immersion in PBS (pH 7.4) at 100°C. Reprinted with permission from Reference 18. © 2017 American Chemical Society. (d) Evolution of the microstructure and surface chemistry associated with the dissolution of Mg in de-ionized (DI) water. (a–d) Optical images; (e–h) scanning electron microscope images with cross-sectional views in the insets. Reprinted with permission from Reference 13. © 2014 Wiley. (e) Dissolution kinetics of bioresorbable materials in aqueous solutions at 37°C. Calculated (lines) and experimental (symbols) results of dissolution studies on (i) Si NMs and (ii) SiO_2 deposited by electron-beam evaporation associated with immersion in aqueous solutions at different pH. Reprinted with permission from Reference 11. © 2014 Wiley. (iii) Change in the resistance of a Mg thin-film resistor as a function of time during dissolution in Hanks' solution at different pH and in DI water. Reprinted with permission from Reference 13. © 2014 Wiley.

hours, as a form of chemical etching and micromachining in alkaline solutions that is widely used in device processing for semiconductor devices and microelectromechanical systems.

By contrast, Si-Ge alloy exhibits a comparatively low rate of dissolution due to a large activation energy (E_A ~0.76 eV), with dissolution rates of only ~2 nm/day in PBS with pH 10 at 37°C.[10] The energy-band structure of Si-Ge alloy provides an explanation for this large difference. Band-bending and the reduced potential barrier at the interface between Si-Ge and solutions with high pH facilitate the formation of a passivating oxide at the alloy surface, resulting in a deceleration in the rate of dissolution.[14] As a semiconductor, Si-Ge can serve as an alternative to monocrystalline Si for applications in high-speed electronics. a-Si is interesting as the basis of thin-film solar cells, due partly to its strong optical absorption across the solar spectrum. Demonstrations of bioresorbable a-Si solar cells show efficiencies, open-circuit voltages, and short-circuit current densities of 4.8%, 0.81 V, and 9.5 mA/cm^2, respectively.[10]

Zinc oxide

Recent studies show that zinc oxide (ZnO), as another inorganic semiconductor for bioresorbable electronics, can also dissolve in water by hydrolysis. ZnO has a wide, direct bandgap (3.37 eV), with large exciton-binding energy (60 meV) and it can be formed with mild solution-based growth conditions, or with various forms of physical and chemical vapor deposition. Relative to Si- and Ge-based semiconductors, ZnO is of additional interest as a lead-free piezoelectric material for mechanical sensing and energy harvesting. Experimental results demonstrate that ZnO films can dissolve to the moderately soluble hydroxide $Zn(OH)_2$ ($ZnO + H_2O \rightarrow Zn(OH)_2$) or to the soluble ion Zn^{2+} ($ZnO + H_2O \rightarrow Zn^{2+} + 20H^-$), depending on the thickness and the volume of the surrounding fluids and other reaction conditions.[15,16] The latter chemistry typically applies to thicknesses of ZnO relevant for thin-film electronics. ZnO formed by sputter deposition dissolves at rate of ~12 nm/h in deionized water (DI; pH 7.4; RT).[16] Such materials can be used as the basis for bioresorbable thin-film transistors (TFTs) with field-effect mobilities of ~0.95 cm^2/Vs, on/off ratios of >10^3, and subthreshold swings of ~1 V/dec (dec [decade] corresponds to a 10× increase of the drain current). These films can also be used in piezoelectric energy harvesters, with peak output power densities and energy-conversion efficiencies in the range of ~10 nW/cm^2 and 0.28%, respectively.[16]

ZnO grown on monocrystalline Si(111) by pulsed laser deposition (PLD) shows a much lower rate of dissolution of ~4 nm/h in PBS (pH 7.4; 37°C) due to its highly (001)-oriented crystal structure and excellent morphological quality (arithmetic surface roughness [R_a] of ~1 nm).[15] These material properties support not only transistors and piezoelectric devices, but also bioresorbable light-emitting diodes (LEDs) when combined with other bioresorbable semiconductors, and with dielectrics and metals.[15] This type of bioresorbable LED emits broadband white light with a maximum optical power density of 0.7 mW/cm^2 at 9 V, with a blue-violet near-band-edge emission and a broad visible emission likely due to defect states. The addition of bioresorbable optical interference filters based on Si NMs yields LEDs with narrow emission profiles at selected wavelengths throughout the visible range.[15]

Indium gallium zinc oxide

Amorphous forms of indium-gallium-zinc oxide (a-IGZO) can be attractive as alternatives to ZnO for TFTs.[17] Recent work shows that indium, gallium, and zinc oxide dissolve to produce zinc hydroxide and indium oxide ($In_2O_3 + 2H_2O \rightarrow 2In(OH)_3$ or $In_2O_3 + H_2O \rightarrow 2InOOH$) by hydrolysis, but the resultant gallium oxide generates insoluble metal hydroxides ($Ga_2O + 4(OH) \rightarrow 2GaO(OH) + H_2O$).[17] Compared to a-Si, a-IGZO offers optical transparency, higher mobility, lower processing temperature, and operational stability. Bioresorbable TFTs with a-IGZO show field-effect mobilities of ~10 cm^2/Vs, on/off ratios of ~2 × 10^6, and subthreshold slopes of ~220 mV/dec, as enhanced properties relative to otherwise similar devices constructed with ZnO or a-Si.[17]

Dielectrics

Additional important materials for bioresorbable electronics are the dielectrics for insulation, passivation, and encapsulation. Previous studies demonstrate that silicon oxides (e.g., SiO_2) and silicon nitrides (e.g., Si_3N_4), frequently used in commercial electronics as interlayers, gate dielectrics, passivation coating, and barriers against water penetration, are also transient in aqueous environments by hydrolysis reactions.[11] Specifically, silicon dioxide (SiO_2) dissolves by ($SiO_2 + 2H_2O \rightarrow Si(OH)_4$), with a chemistry that is similar to that of Si (Figure 1c).[18] The rate of dissolution in PBS (pH 7.4; 37°C) is, in general, much lower than that for Si, depending on the methods for deposition and growth, and resultant material density or stoichiometry.[11] For example, oxides thermally grown (tg) in O_2 (tg-dry) and H_2O vapor (tg-wet) show rates of 0.003 and 0.01 nm/day, respectively. The rates of oxides formed by plasma-enhanced chemical vapor deposition (PECVD) and electron-beam evaporation (e-beam) are ~0.1 and ~10 nm/day, respectively. The tg-dry and PECVD oxides are close to stoichiometric (i.e., Si:O = 1:2), while those deposited by e-beam evaporation are typically oxygen rich, at $SiO_{2.2}$ (i.e., Si:O = 1:2.2). The very low rate of dissolution for tg-dry oxide follows from its relatively high density (2.34 g/cm^3) and favorable stoichiometry (Si:O = 1:2). By comparison, e-beam oxide, which has a relatively low density (1.9 g/cm^3) and nonstoichiometric chemistry (Si : O = 1:2.2), shows a comparatively high rate.[11] As with silicon, the rates increase with pH, due to the role of OH– in the hydrolysis process, as shown in Figure 1e(ii). Accelerated dissolution also occurs in the presence of divalent cations (e.g., Ca^{2+}). The Ca^{2+} may have an increased ability to deprotonate surface silanol groups formed by the absorption of water, or to enhance the reactivity of water and siloxane groups as suggested in previous studies.[18,19]

For silicon nitrides, hydrolysis occurs through two steps (1) oxidation into silicon oxide ($Si_3N_4 + 6H_2O \rightarrow 3SiO_2 + 4NH_3$); and (2) hydrolysis of silicon oxide into silicic acid ($SiO_2 + 2H_2O \rightarrow Si(OH)_4$).[11] Since SiO_2 is an intermediate product of the hydrolysis of silicon nitrides, the dissolution rate for this material depends on pH in a manner similar to that of SiO_2. As previously discussed, the method of deposition affects the density and stoichiometry and therefore the hydrolysis kinetics. In PBS (pH 7.4; 37°C), silicon nitride formed by low-pressure chemical vapor deposition (LPCVD) exhibits a dissolution rate (0.16 nm/day) that is lower than that of silicon nitride formed by PECVD (0.85 nm/day), primarily because the latter has a more favorable stoichiometry (Si:N = 3:3.9) and a higher density (3.1 g/cm^3) than the former (Si:N = 3:3.3; 2.5 g/cm^3).[11]

Both silicon oxides and silicon nitrides are useful as gate dielectrics in transistors, as insulators in capacitors, and as interlayers for electrical interconnects. Recent studies also demonstrate their utility as bioresorbable encapsulation layers, where they serve as biofluid barriers to define stable periods of operation for the underlying electronics.[20,21] For example, a bioresorbable pressure sensor encapsulated by a ~10-nm-thick layer of SiO_2 operates without drift for 3 h and then dissolves rapidly during immersion in PBS at 95°C, corresponding to a lifetime, projected by Arrhenius scaling, of 57 weeks.[20] Organic polymers do not function well in this type of application due to the permeability of water through these classes of materials.

Electrical conductors

The third main type of material in electronics is the conductor. Here, inorganic options include magnesium (Mg), zinc (Zn), tungsten (W), iron (Fe), and molybdenum (Mo) as thin films or composites with bioresorbable polymers.[13,22] Figure 1d presents a series of optical micrographs of patterned thin films of Mg at various times of immersion in DI water at room temperature (RT), indicating that a 300-nm-thick layer of Mg dissolves within three days under these conditions. The chemistry of dissolution for these metals also involves hydrolysis (e.g., $Mg + 2H_2O \rightarrow Mg(OH)_2 + H_2$; $Zn + 2H_2O \rightarrow Zn(OH)_2 + H_2$; $2W + 2H_2O + 3O_2 \rightarrow 2H_2WO_4$; $2Mo + 2H_2O + 3O_2 \rightarrow 2H_2MoO_4$), although at rates that are much higher than those for inorganic semiconductors and dielectrics immersed in PBS (pH 7.4; 37°C): ~1700 nm/day (deposited Mg); ~3500 nm/day (Zn foil); ~150 nm/day (W foil); ~80 nm/day (Fe foil); ~20 nm/day (Mo foil).[13,22] In all cases, an oxide layer forms immediately after exposure of a fresh metallic surface to oxygen in the atmosphere. In addition, oxides as well as the end products of dissolution, such as $Mg(OH)_2$, appear on the surfaces and increase in thickness due to the hydration of the native oxide followed by a dissolution-precipitation mechanism. These layers can serve as partially protective coatings to slow the dissolution of underlying metal. In the case of Fe, measuring a specific degradation rate is difficult because its reaction products (Fe_2O_3 and Fe_3O_4) have very low solubility and induce irregular and inhomogeneous dissolution.

Metallic alloys can also be of interest. For example, Mg-Zn alloy (AZ31B) dissolves at a rate of 480 nm/day in DI water at RT, intermediate between the rates for Mg and Zn. Figure 1e(iii) illustrates changes in the resistance of a serpentine structure of Mg (300-nm thick) in DI water and Hanks' solution (pH 5, 7.4, and 8 at RT, and pH 7.4 at 37°C). The changes in resistance occur at particularly high rates in Hanks' solution (a balanced salt solution composed of inorganic salts and supplemented with glucose), likely due to the presence of chlorides (Cl^-) that promote rapid chemical attack, as reported in corrosion studies of mass loss in bulk samples of Mg.[23] The weak dependence on pH between pH 5 and pH 8 is consistent with the findings for bulk Mg alloys.[24] Both AZ31B and Zn show similar trends in pH dependence. Mo exhibits faster changes in resistance during immersion in DI water or at low pH than those in Hanks' solution or at high pH, due to the strong dependence of Mo dissolution on oxygen solubility in aqueous solution. The presence of ions and increasing basicity is known to reduce oxygen solubility.[13]

Figure 2 summarizes the rates of dissolution for these metals and other classes of inorganic electronic materials in PBS (pH 7.4; 37°C). Of note is the strong dependence of the rates on many aspects of the chemical composition of the surrounding fluids, some fraction of which cannot be predicted accurately based on underlying models of the chemical reaction kinetics. In addition, modes of degradation can involve not only dissolution from the top surfaces of the materials, but also by reactive diffusion, fragmentation, interfacial failure, and other mechanisms. As a result, the development of engineering designs for specific applications demands empirical measurements of the rates of degradation under conditions of interest.

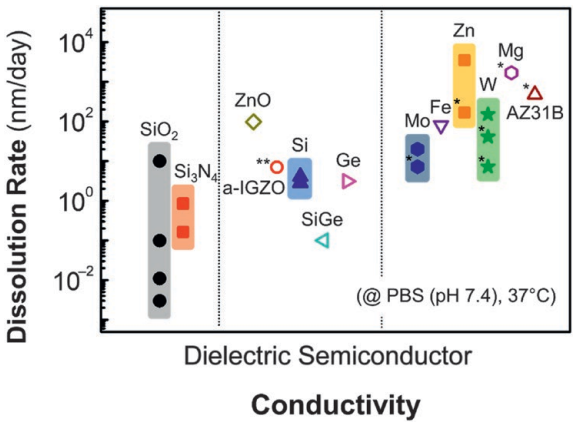

Figure 2. A summary plot of the rates of dissolution of bioresorbable inorganic dielectric, semiconductor, and conductor (metal) materials. These data result from tests that involve immersion in phosphate buffer solution (PBS) at a pH of 7.4 and temperature of 37°C. Entries marked * and ** correspond to measurements in different conditions: (*) in de-ionized water (RT); (**) in bovine serum (37°C). The results for a-IGZO correspond to dissolution to the stage that only gallium-based compounds remain.

Materials aspects of biocompatibility

The biocompatibility of bioresorbable inorganic materials (and the products of their dissolution by hydrolysis) is a critically important consideration in the context of the applications considered here. In the case of Si NMs, the main reaction product, silicic acid ($Si(OH)_4$), is a nontoxic small molecule that represents the most common form of bioavailable silicon in the human body (serum contains 11–25 μg silicon/dL), and it is a recommended part of a daily diet. According to the literature, silicic acid does not accumulate within the body, but is absorbed by the gastrointestinal tract and is excreted via the urinary pathway.[20,25]

As an example of a study of biocompatibility, **Figure 3**a shows results obtained from *in vivo* analysis of a bioresorbable optical sensor built entirely with inorganic materials—tg-SiO_2 (~10 nm), Si NMs (250 nm), adhesion layers of amorphous silica (~200 nm), and a slab of silicon with a square cavity (dimensions, 750 μm × 750 μm × 10 μm; cavity area, 250 μm × 250 μm).[21] Histopathologic evaluation of tissue samples obtained from the brain, heart, kidney, liver, lung, and spleen collected from a mouse with a sensor implanted in the brain for five weeks and a control mouse without an implant reveals no significant inflammation, ischaemia/tissue necrosis, or other architectural/histologic abnormalities in the major organs of both groups of mice, either grossly or by microscopic examination.[21]

Investigations of elemental biodistribution reveal additional effects, as shown in Figure 3b for the case of Si (left) and Zn (right) associated with a bioresorbable spectrometer that includes a Si NM photodetector (length × width × thickness: 500 μm × 500 μm × 1500 nm), two Zn electrodes (length × width × thickness: 10,000 μm × 200 μm × 400 nm) and a poly(lactic-*co*-glycolic acid) fiber waveguide (diameter: ~150 μm; length: 10,000 μm).[26] The results include the concentrations of Si and Zn in the blood, brain, heart, kidney, liver, lung, muscle, and spleen tissues explanted from control mice and mice with an implanted device at one, three, five, and seven weeks after implantation. Elevated concentrations of Si and Zn appear during the first three weeks in the blood, heart, muscle, and spleen for Si, and the heart, lung, and muscle for Zn, then gradually recover to within a normal range within seven weeks. No abnormal accumulation of Si and Zn appears in any tissues during the seven-week implantation period. The slow increase of concentrations of Si and Zn in the kidneys (from week one to week five for Si, and from week one to week seven for Zn) suggest renal clearance to maintain the metabolic balance of these materials. The hematology (complete blood count) and the blood chemistry also provide insights. Analysis of complete blood counts and blood chemistry tests for this same photodetector system show no sign of organ damage or injury, and no change in the electrolyte or enzyme balance (Figure 3c).[26]

High-resolution cross-sectional images of the implantation site with immunohistochemical staining provide additional evidence of the biocompatibility of these inorganic electronic materials. Figure 3d shows that the device induces some minimal inflammatory glial responses (day one) in brain tissue, but that these gradually decrease over time to a level comparable to the control group, suggesting normal recovery from the implantation surgery.[26] The viability of the surrounding neurons and glia remain unchanged compared to that of the control group. The cross-sectional area of the implant decreases over time, consistent with continuous bioresorption without adverse effect on the neighboring neurons. The morphologies of the soma, dendrites and axons of the experimental group (days 1, 7, and 14) are similar to those of the control group, indicating minimal physiological effects on the surrounding neural and glial networks.[26] Studies based on chronic implantation of Si-based electrodes in brain tissue for six months also support a similar conclusion, without toxic reaction.[27,28]

Biomedical applications of bioresorbable electronics

Traditional, permanent electronic implants offer diverse and essential functions in research on living systems and in many forms of medical diagnostics and treatment. The concept of bioresorbable implants creates new opportunities for engineered systems in which the operational lifetimes match those of a targeted biological process such as wound healing. These devices simply disappear after they are no longer needed, thereby eliminating the costs and risks associated with secondary surgical extraction procedures, otherwise necessary to eliminate device load on the patient and associated risks of uncontrolled migration and infection.[29–31] The following summarizes recent research demonstrations of these classes of devices, across a range of potential uses in medicine, where the essential functional materials are all inorganic and the supporting substrates, encapsulants, and other elements use organic polymers.

The first example is in neurophysiologic monitoring, as commonly used for diagnosing and treating brain disorders such as epilepsy, Parkinson's disease, depression, and chronic pain. **Figure 4**a shows passively and actively addressed bioresorbable systems for electrophysiological monitoring on the surface of the brain.[32] In the simplest case, highly doped Si NMs serve as bioresorbable neural interfaces, whose slow, controlled surface erosion mode of bioresorption is attractive relative to that of bioresorbable metals, which undergo comparatively fast dissolution kinetics, with a tendency to crack, fragment, and flake during the process. In these platforms, small, passively addressed collections of Si NM electrodes record normal physiologic and epileptic activity in electrocorticography (ECoG) and subdermal encephalography (EEG), both in acute and chronic situations. The slow rates of dissolution in biofluids allow for stable use for periods up to ~30 days *in vivo*. More advanced systems are possible by the inclusion of backplane electronics composed of Si NM transistors for active multiplexing in high-speed, high-resolution mapping schemes, with multilayer constructs that include interlayer dielectrics and other features.[32]

Figure 4b summarizes another example, in the form of a bioresorbable intracranial pressure (ICP) sensor, designed for monitoring recovery following a traumatic injury to the brain,

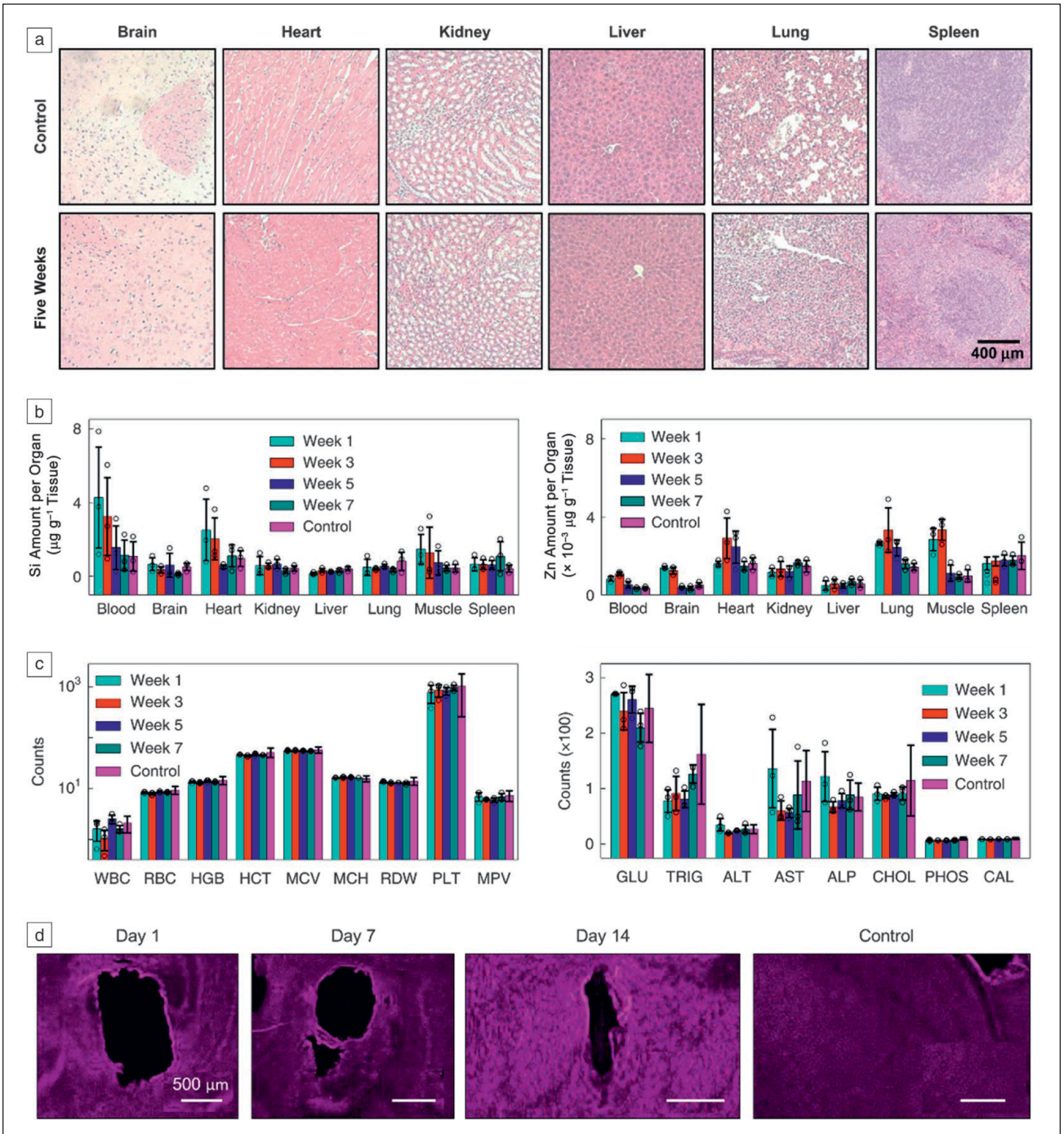

Figure 3. Biocompatibility of bioresorbable inorganic electronic materials and devices built with them. (a) Representative histological results from various organs collected five weeks after implantation of a bioresorbable pressure sensor constructed with SiO_2 and Si. Reprinted with permission from Reference 21. © 2019 AAAS. (b) *In vivo* biodistribution of key elements (Si [left] and Zn [right]) of bioresorbable photonic devices for spectroscopic characterization of biological tissues. Implantation was in the subcutaneous region near the flank region, and comparisons were made with control animals. (c) Analysis of complete blood counts and blood chemistry for the mice in (b). Note: ALP, alkaline phosphatase; ALT, alanine aminotransferase; AST, aspartate transaminase; CAL, calcium; CHOL, cholesterol; GLU, glucose; HCT, hematocrit level; HGB, blood hemoglobin level; MCH, mean corpuscular hemoglobin; MCV, mean corpuscular volume; MPV, mean platelet volume; PHOS, phosphorus; PLT, platelet count in blood; RBC, red blood cell; RDW, red cell distribution width; TRIG, triglycerides; WBC, white blood cell. (d) Representative confocal images of 30-μm horizontal striatal slices at various stages after implantation of the bioresorbable optical probes, compared with a control group. The images show cross-sectional views of the implantation site (black) with immunohistochemical staining for Nissl bodies (neurotrace, purple). (b–d) Reprinted with permission from Reference 26. © 2019 Nature Publishing Group.

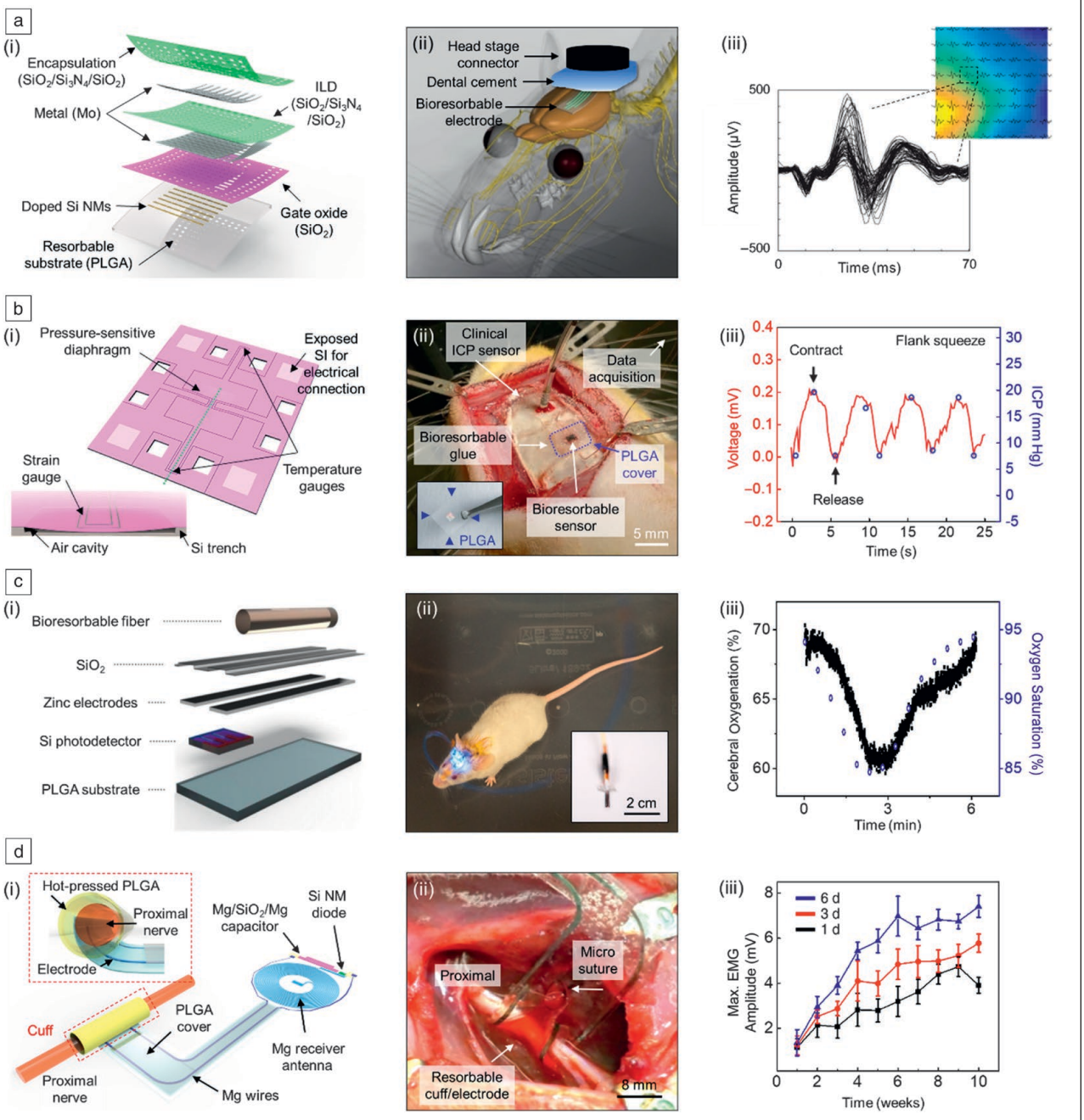

Figure 4. Biomedical devices built with inorganic bioresorbable electronic materials. (a) Bioresorbable actively multiplexed electrode array for electrocorticography (ECoG). (i) Schematic illustration of the device. (ii) Cartoon illustration of a four-channel bioresorbable electrode array implanted on the left hemisphere of the brain of a rat, for chronic recordings. (iii) Temporal characteristics and spatial distributions of electrical potentials evoked by stimulation. Reprinted with permission from Reference 32. © 2016 Nature Publishing Group. (b) Bioresorbable sensor of intracranial pressure (ICP) and temperature (ICT). (i) Schematic illustration of a bioresorbable ICP/T sensor. Si NM strain gauges on a flexible diaphragm capture pressure variations via the piezoresistive response of the silicon. Temperature gauges react to temperature changes via temperature-dependent resistance. (ii) Photograph of a bioresorbable ICP sensor, mounted on a thin film of PLGA (~10-μm thick; inset), implanted device-side down in the intracranial cavity of a rat. (iii) *In vivo* monitoring of variations in ICP. Reprinted with permission from Reference 20. © 2019 Nature Publishing Group. (c) Bioresorbable photodetector with a bioresorbable fiber optic probe for spectroscopic characterization of biological tissues. (i) Schematic illustration of the device. (ii) Image of a mouse implanted with a device. The inset provides an enlarged view of the active sensing region. (iii) Comparison of cerebral oxygenation measured by a bioresorbable spectrometer and a commercial sensor. Reprinted with permission from Reference 26. © 2019 Nature Publishing Group. (d) Bioresorbable, wireless electrical stimulator for peripheral nerve regeneration. (i) Schematic illustration of the design. (ii) Surgical implantation of a stimulator on the sciatic nerve in a rodent model. (iii) Time dependence of maximum electromyography (EMG) amplitude measured from the tibialis anterior muscle after a transection injury of the sciatic nerve with electrical stimulation for 1 h a day for one, three, and six days. Reprinted with permission from Reference 34. © 2018 Nature Publishing Group. Note: ILD, interlayer dielectrics; PLGA, poly(lactic-*co*-glycolic acid).

with lifetimes of several days to several weeks.[20] The most recent embodiment, following an initial demonstration,[33] incorporates a Si NM piezoresistive strain sensor encapsulated by SiO_2 as a top seal on an underlying cavity. Changes in the pressure of surrounding cerebrospinal fluids induce deflections of the membrane and corresponding changes in resistance of the strain gauge, for electrical readout in a Wheatstone bridge configuration to convert the resistance into a voltage. Thermally grown layers of SiO_2 form barriers that prevent interactions with biofluids throughout the desired monitoring period, but with thicknesses sufficiently small to allow complete bioresorption within a reasonable time frame, typically less than a year. Studies using rodent models indicate capabilities for stable, accurate measurements of temperature and pressure in the intracranial space for 25 days.[20]

Bioresorbable photonic devices are also possible, for real-time monitoring of internal physiological processes to inform pharmacological drug delivery schedules, surgical intervention procedures, or the management of recovery and rehabilitation. Figure 4c shows a schematic illustration of a device that consists of three bioresorbable components—a polymer fiber, a Si photodetector, and a Zn electrode and interconnect.[26] Deploying these bioresorbable spectrometers in live animal models (Figure 4c[ii]) demonstrates possibilities in sensing of cerebral temperature, cerebral oxygen saturation (Figure 4c[iii]), and neural activity continuously as the animals move in cage environments.[26]

In addition to monitoring, bioresorbable electronic systems can be used for various forms of therapy. For example, diodes, capacitors, and RF coils form the basis of bioresorbable wirelessly powered and wirelessly controlled nerve stimulators, as shown in Figure 4d.[34] Here, an RF power harvester and an electrical interface to a targeted peripheral nerve (Figure 4d[i]) can deliver stimulation in a controlled manner using an external source of RF power. The harvester consists of a loop antenna with a bilayer, dual-coil configuration (Mg, ~50-μm thick), an RF diode based on a doped Si NM with Mg electrodes, and a parallel plate capacitor that uses Mg conducting planes (~50-μm thick) above and below a layer of SiO_2 (~600-nm thick). Constituent materials completely disintegrate and dissolve within 25 days. Minimal inflammatory responses and fibrosis occur over an eight-week monitoring period, with no evidence of axonal injury or damage at the nerve–cuff interface. Figure 4d(iii) demonstrates enhanced therapeutic effects associated with multiple days of stimulation (six days) during the process of healing of a damaged peripheral nerve, enabled by this implantable, bioresorbable stimulator. Modified versions of this same platform can address a range of clinical scenarios and target tissues/organ systems, including the brain and spinal cord, skeletal muscles, and cardiac tissues with relatively few modifications to the form factor and the interfacial electrode sites.[34]

Conclusions

Knowledge of the chemistry associated with bioresorbable inorganic electronic materials forms the scientific foundations for high-performance classes of transient electronics generally, and bioresorbable electronics more specifically. Interest in this area derives mainly from the broad potential utility of this technology in medical systems and in other areas such as environmental monitoring and biological research. Recent published results highlighted in this article identify various types of bioresorbable inorganic materials that offer both biocompatibility and high-performance electronic properties as semiconductors, dielectrics, and conductors. Platforms for most practical applications combine these materials with bioresorbable polymers as substrates, encapsulation layers, and sensing components to form working systems, with stable operating lifetimes over timeframes of interest in biomedicine and, in some examples, with unusual characteristics such as mechanical stretchability to facilitate biointegration with soft tissues.[35]

From a materials perspective, the methods of deposition, alloy compositions, doping/impurity levels, and other materials-related parameters determine the dissolution rates and other device characteristics, including methods for actively triggering or controlling the processes of bioresorption. Significant opportunities exist in exploring additional bioresorbable electronic materials, particularly those with properties that can support optoelectronic functionality and advanced operation in biochemical sensing. These and other research directions, from fundamental studies of the material chemistry to innovative materials engineering of the devices and systems, together with the important applications that will follow from successful efforts, suggest a bright future for this field.

References

1. S.-W. Hwang, H. Tao, D.-H. Kim, H. Cheng, J.-K. Song, E. Rill, M.A. Brenckle, B. Panilaitis, S.M. Won, Y.-S. Kim, Y.M. Song, K.J. Yu, A. Ameen, R. Li, Y. Su, M. Yang, D.L. Kaplan, M.R. Zakin, M.J. Slepian, Y. Huang, F.G. Omenetto, J.A. Rogers, *Science* **337**, 1640 (2012).
2. S.K. Kang, J. Koo, Y.K. Lee, J.A. Rogers, *Acc. Chem. Res.* **51**, 988 (2018).
3. M.A. Yoder, Z. Yan, M. Han, J.A. Rogers, R.G. Nuzzo, *J. Am. Chem. Soc.* **140**, 9001 (2018).
4. V.R. Feig, H. Tran, Z. Bao, *ACS Cent. Sci.* **4**, 337 (2018).
5. L. Yin, A.B. Farimani, K. Min, N. Vishal, J. Lam, Y.K. Lee, N.R. Aluru, J.A. Rogers, *Adv. Mater.* **27**, 1857 (2015).
6. S.W. Hwang, G. Park, H. Cheng, J.K. Song, S.K. Kang, L. Yin, J.H. Kim, F.G. Omenetto, Y. Huang, K.M. Lee, J.A. Rogers, *Adv. Mater.* **26**, 1992 (2014).
7. H. Cheng, *J. Mater. Res.* **31**, 2549 (2016).
8. Y.K. Lee, K.J. Yu, E. Song, A. Barati Farimani, F. Vitale, Z. Xie, Y. Yoon, Y. Kim, A. Richardson, H. Luan, Y. Wu, X. Xie, T.H. Lucas, K. Crawford, Y. Mei, X. Feng, Y. Huang, B. Litt, N.R. Aluru, L. Yin, J.A. Rogers, *ACS Nano* **11**, 12562 (2017).
9. S.W. Hwang, D.H. Kim, H. Tao, T. Il Kim, S. Kim, K.J. Yu, B. Panilaitis, J.W. Jeong, J.K. Song, F.G. Omenetto, J.A. Rogers, *Adv. Funct. Mater.* **23**, 4087 (2013).
10. S.K. Kang, G. Park, K. Kim, S.W. Hwang, H. Cheng, J. Shin, S. Chung, M. Kim, L. Yin, J.C. Lee, K.M. Lee, J.A. Rogers, *ACS Appl. Mater. Interfaces* **7**, 9297 (2015).
11. S.K. Kang, S.W. Hwang, H. Cheng, S. Yu, B.H. Kim, J.H. Kim, Y. Huang, J.A. Rogers, *Adv. Funct. Mater.* **24**, 4427 (2014).
12. R. Li, H. Cheng, Y. Su, S.W. Hwang, L. Yin, H. Tao, M.A. Brenckle, D.H. Kim, F.G. Omenetto, J.A. Rogers, Y. Huang, *Adv. Funct. Mater.* **23**, 3106 (2013).
13. L. Yin, H. Cheng, S. Mao, R. Haasch, Y. Liu, X. Xie, S.W. Hwang, H. Jain, S.K. Kang, Y. Su, R. Li, Y. Huang, J.A. Rogers, *Adv. Funct. Mater.* **24**, 645 (2014).
14. J.T. Borenstein, N.D. Gerrish, M.T. Currie, E.A. Fitzgerald, *IEEE Int. Microelectromech. Syst. Conf. Tech. Dig.* (1999), p. 205.
15. D. Lu, T. Liu, J. Chang, D. Peng, Y. Zhang, J. Shin, T. Hang, W. Bai, Q. Yang, J.A. Rogers, *Adv. Mater.* **31**, 1902739 (2019).

16. C. Dagdeviren, S.W. Hwang, Y. Su, S. Kim, H. Cheng, O. Gur, R. Haney, F.G. Omenetto, Y. Huang, J.A. Rogers, *Small* **9**, 3398 (2013).
17. S.H. Jin, S.K. Kang, I.T. Cho, S.Y. Han, H.U. Chung, D.J. Lee, J. Shin, G.W. Baek, T. Il Kim, J.H. Lee, J.A. Rogers, *ACS Appl. Mater. Interfaces* **7**, 8268 (2015).
18. Y.K. Lee, K.J. Yu, Y. Kim, Y. Yoon, Z. Xie, E. Song, H. Luan, X. Feng, Y. Huang, J.A. Rogers, *ACS Appl. Mater. Interfaces* **9**, 42633 (2017).
19. P.V. Brady, J.V. Walther, *Chem. Geol.* **82**, 253 (1990).
20. J. Shin, Y. Yan, W. Bai, Y. Xue, P. Gamble, L. Tian, I. Kandela, C.R. Haney, W. Spees, Y.K.Y. Lee, M. Choi, J. Ko, H. Ryu, J.K. Chang, M. Pezhouh, S.K. Kang, S.M. Won, K.J. Yu, J. Zhao, Y.K.Y. Lee, M.R. MacEwan, S.K. Song, Y. Huang, W.Z. Ray, J.A. Rogers, *Nat. Biomed. Eng.* **3**, 37 (2019).
21. J. Shin, Z. Liu, W. Bai, Y. Liu, Y. Yan, Y. Xue, I. Kandela, M. Pezhouh, M.R. MacEwan, Y. Huang, W.Z. Ray, W. Zhou, J.A. Rogers, *Sci. Adv.* **5**, 1 (2019).
22. S.K. Kang, S.W. Hwang, S. Yu, J.H. Seo, E.A. Corbin, J. Shin, D.S. Wie, R. Bashir, Z. Ma, J.A. Rogers, *Adv. Funct. Mater.* **25**, 1789 (2015).
23. G. Song, A. Atrens, *Adv. Eng. Mater.* **5**, 837 (2003).
24. R. Ambat, N.N. Aung, W. Zhou, *J. Appl. Electrochem.* **30**, 865 (2000).
25. D.M. Reffitt, R. Jugdaohsingh, R.P.H. Thompson, J.J. Powell, *J. Inorg. Biochem.* **76**, 141 (1999).
26. W. Bai, J. Shin, R. Fu, I. Kandela, D. Lu, X. Ni, Y. Park, Z. Liu, T. Hang, D. Wu, Y. Liu, C.R. Haney, I. Stepien, Q. Yang, J. Zhao, K.R. Nandoliya, H. Zhang, X. Sheng, L. Yin, K. MacRenaris, A. Brikha, F. Aird, M. Pezhouh, J. Hornick, W. Zhou, J.A. Rogers, *Nat. Biomed. Eng.* **3**, 644 (2019).
27. S. Schmidt, K. Horch, R. Normann, *J. Biomed. Mater. Res.* **27**, 1393 (1993).
28. B.W. Kristensen, J. Noraberg, P. Thiébaud, M. Koudelka-Hep, J. Zimmer, *Brain Res.* **896**, 1 (2001).
29. T. Hamaoka, K.K. McCully, M. Niwayama, B. Chance, *Philos. Trans. A Math. Phys. Eng. Sci.* **369**, 4591 (2011).
30. M. Ferrari, V. Quaresima, *Neuroimage* **63**, 921 (2012).
31. S. Lloyd-Fox, A. Blasi, C.E. Elwell, *Neurosci. Biobehav. Rev.* **34**, 269 (2010).
32. K.J. Yu, D. Kuzum, S.W. Hwang, B.H. Kim, H. Juul, N.H. Kim, S.M. Won, K. Chiang, M. Trumpis, A.G. Richardson, H. Cheng, H. Fang, M. Thompson, H. Bink, D. Talos, K.J. Seo, H.N. Lee, S.K. Kang, J.H. Kim, J.Y. Lee, Y. Huang, F.E. Jensen, M.A. Dichter, T.H. Lucas, J. Viventi, B. Litt, J.A. Rogers, *Nat. Mater.* **15**, 782 (2016).
33. S.K. Kang, R.K.J. Murphy, S.W. Hwang, S.M.S.H. Lee, D.V. Harburg, N.A. Krueger, J. Shin, P. Gamble, H. Cheng, S. Yu, Z. Liu, J.G. McCall, M. Stephen, H. Ying, J. Kim, G. Park, R.C. Webb, C.H. Lee, S. Chung, D.S. Wie, A.D. Gujar, B. Vemulapalli, A.H. Kim, K.M. Lee, J. Cheng, Y. Huang, S.M.S.H. Lee, P.V. Braun, W.Z. Ray, J.A. Rogers, *Nature* **530**, 71 (2016).
34. J. Koo, M.R. MacEwan, S.-K.K. Kang, S.M. Won, M. Stephen, P. Gamble, Z. Xie, Y. Yan, Y.-Y.Y. Chen, J. Shin, N. Birenbaum, S. Chung, S.B. Kim, J. Khalifeh, D.V. Harburg, K. Bean, M. Paskett, J. Kim, Z.S. Zohny, S.M. Lee, R. Zhang, K. Luo, B. Ji, A. Banks, H.M. Lee, Y. Huang, W.Z. Ray, J.A. Rogers, *Nat. Med.* **24**, 1830 (2018).
35. S.W. Hwang, C.H. Lee, H. Cheng, J.W. Jeong, S.K. Kang, J.H. Kim, J. Shin, J. Yang, Z. Liu, G.A. Ameer, Y. Huang, J.A. Rogers, *Nano Lett.* **15**, 2801 (2015).□

Yeonsik Choi is a postdoctoral researcher in the Center for Bio-Integrated Electronics at Northwestern University. He obtained his BS degree in 2009, and his MS degree in 2011 from Yonsei University, Republic of Korea, in materials science and engineering. He received his PhD degree in 2019 in materials science from the University of Cambridge, UK. He was a senior researcher from 2011 to 2015 with the Advanced Materials Development Team at LG Chem Ltd., Republic of Korea. Choi can be reached by email at yeonsik.choi@northwestern.edu.

Jahyun Koo is a postdoctoral researcher in the Center for Bio-Integrated Electronics at Northwestern University. He received his BS and MS degrees in nuclear and quantum engineering from the Korea Advanced Institute of Science and Technology (KAIST), Republic of Korea, in 2010 and 2012, respectively. He received his PhD degree in materials science and engineering from KAIST in 2017. His research interests include bioresorbable devices and implantable electronics. Koo can be reached by email at nano.jhkoo@gmail.com.

John A. Rogers is the Louis Simpson and Kimberly Querrey Professor of Materials Science and Engineering, Biomedical Engineering and Medicine, and the director of the Institute for Bioelectronics at Northwestern University. His awards include a MacArthur Fellowship in 2009, the Lemelson-MIT Prize in 2011, the Materials Research Society Medal in 2018, and the Benjamin Franklin Medal in 2019. He is a member of the National Academy of Engineering, the National Academy of Sciences, the National Academy of Medicine, and the American Academy of Arts & Sciences. Rogers can be reached by email at jrogers@northwestern.edu.